Polymer–Polymer Interactions in Dilute Solution

P. M. Cotts*

IBM Research Division, Almaden Research Center, 650 Harry Road, San Jose, California 95120-6099

J. C. Selser

Department of Physics, University of Nevada, Las Vegas, Nevada 89154.
Received July 22, 1989; Revised Manuscript Received October 16, 1989

ABSTRACT: Coil–coil interactions in dilute solution for poly(α-methylstyrene) in sub-Θ, Θ, marginal, and good solvents were studied using static and dynamic light scattering. The behavior observed across the solvent quality range is well described by a semiempirical fit to the interchain parameter k_D^{φ} versus the reduced radius $X \equiv \bar{S}/R_H$ using a recent theoretical treatment developed by Akcasu and co-workers.

I. Introduction

Light scattering is an elegant and noninvasive method of investigating polymer–polymer interactions in dilute solution. This paper presents the results of a light-scattering study of PαMS–PαMS (poly(α-methylstyrene)) interactions in good, marginal, Θ, and sub-Θ solvents.

When time-averaged or static light scattering is used, the polymer weight-averaged molecular weight, $\bar{M}_W$, and the solution second virial coefficient, A_2, can be determined, while dynamic light scattering (specifically photon correlation spectroscopy, PCS) provides the hydrodynamic radius, R_H, along with the concentration coefficient, k_D^c [1-3]

$$D(c) = D_0(1 + k_D^c c + ...) \tag{1}$$

$$D_0 = kT/6\pi\eta_0 R_H \tag{2}$$

where mutual diffusion coefficients $D(c)$ are determined from measured autocorrelation functions. As the fluctuations in scattering intensity arise from the random formation and relaxation of concentration gradients in the solution, the concentration dependence contains both thermodynamic and transport or hydrodynamic factors. The Gibbs–Duhem equation permits expression of the concentration dependence of $D(c)$ as

$$D(c) = \frac{M}{N_A f(c)}(1 - \bar{v}c)\frac{\partial \pi}{\partial c} \tag{3a}$$

or

$$D(c) = \frac{kT}{f(c)}(1 - \bar{v}c)(1 + 2A_2Mc + ...) \tag{3b}$$

where the osmotic compressibility ($\partial\pi/\partial c$), which may be obtained from time-averaged light scattering, has been expanded in a virial series including the second virial coefficient, A_2, and molecular weight, M, explicitly. The thermodynamic and hydrodynamic parameters incorporated in k_D are then related according to

$$k_D^c = 2A_2M - k_s^c - \bar{v} \tag{4}$$

expressed in concentration units. The polymer partial specific volume in solution is $\bar{v}$, while k_s^c is the linear term in the concentration expansion for the friction coefficient

$$f(c) = f_0(1 + k_s^c c + ...) \tag{5}$$

with c the solution concentration. Theoretical calculations use the volume fraction, ϕ, where

$$\phi = cN_A V_H/M \tag{6}$$

with the hydrodynamic volume, V_H, given by

$$V_H = (4/3)\pi R_H^3 \tag{7}$$

Recast in volume fraction units and ignoring the negligible contribution of $\bar{v}$ to k_D^{φ} for large polymers, eq 4 reads

$$k_D^{\varphi} = 8X^3 - k_s^{\varphi} \tag{8}$$

with $X \equiv \bar{S}/R_H$ and $\bar{S}$ defined as an effective hard-sphere radius determined by the second virial coefficient, A_2 [4]

$$\bar{S} = (3M^2A_2/16\pi N_A)^{1/3} \tag{9}$$

and N_A Avogadro's number.

The thermodynamic excluded-volume term in eq 8, $8X^3$, may be measured by intensity light scattering or colligative methods and is positive in thermodynamically good solvents; decreasing to zero at T_θ and becoming negative below T_θ. The hydrodynamic term, k_s^{φ}, has been the focus of several earlier theories.[4-7] While these transport theories differ in their quantitative predictions of k_s^{φ}, they all predict that k_s^{φ} remains positive even at T_θ so that k_D^{φ} is expected to be negative at T_θ, as has been observed experimentally. Accurate measurements of k_D^{φ} are more accessible than measurements of k_s^{φ} from transport properties such as sedimentation or tracer diffusion. An especially compact and useful way of employing k_D^{φ}, $\bar{S}$, and R_H in the study of polymer–polymer interactions in dilute solution has recently been developed by Akcasu and Benmouna[8] and by Akcasu and Han,[9,10] and this method is used to develop the principal conclusions of the present study. The Akcasu theory differs from the earlier transport theories for k_s^{φ} in that both the thermodynamic and hydrodynamic contributions to k_D^{φ} are evaluated from the static structure factor obtained from light scattering. In this method, experimentally determined values of k_D^{φ} are plotted against experimentaly determined values of X over a range of polymer molecular weights and for several solution solvent qualities, which may be varied by varying solvent or temperature. Note that both the temperature and the polymer molecular weight dependences of k_D^{φ} are incorporated in X.[10]

0024-9297/90/2223-2050$02.50/0

Table I
PαMS Molecular Weight Results

sample no.	$\bar{M}_W \pm 6\%$	$\bar{M}_W/\bar{M}_N$ (SEC)
1	6 300	1.35
2	24 600	1.17
3	71 000	1.09
4	109 300	1.09
5	293 000	1.08
6	584 000	1.14
7	726 000	1.16
8	1 010 000	1.14
9	2 900 000	1.18

Theoretical treatments of solution binary polymer interactions may then be tested by formulating k_s^{φ} as a function of X and comparing the observed dependence of k_D^{φ} on X with that predicted by eq 8.

II. Experimental Section

Nine samples of poly(α-methylstyrene) (PαMS) with molecular weights in the range 6×10^3–3×10^6 were used in this study (see Table I). These samples were prepared by anionic polymerization at the Pressure Chemical Co.; relative amounts of the different tactic forms as determined by ^{1}H or ^{13}C NMR were 46 ± 6% isotactic plus heterotactic and 53 ± 6% syndiotactic.[11] The fraction of isotactic triads was very small, 5 ± 2%. These values are very similar to those reported by Kato and co-workers[12] for anioncally polymerized samples of PαMS. The steric hindrance toward isotactic addition is evident although the fraction of syndiotactic is similar to the smallest values reported for a variety of syntheses.[13] The fraction of syndiotactic triads was somewhat larger at lower molecular weights as was also reported by Kato and co-workers.[12] Stock solutions for light scattering were prepared gravimetrically at room temperature in spectrophotometric-grade toluene and at 50 °C in spectrophotometric-grade cyclohexane. Samples of reduced concentration were prepared by serial dilution of the stock solution and filtered through 0.5-μm Fluoropore filters directly into cells that had been cleaned by refluxing in an isopropyl alcohol drier. Light-scattering measurements were then made at 25, 34.5, and 50 °C in cyclohexane (sub-Θ, Θ, and marginal solvents)[12,15,17] and at 25 °C in toluene (good solvent; see ref 16 and below).

During measurement, samples were maintained within 0.05 °C of the reported temperatures by thermostatic control. Static light-scattering measurements were made either in a Chromatix KMX-6 low-angle laser light-scattering photometer or in a Brookhaven BI-2030 light-scattering photometer. PCS measurements were made either in the Brookhaven photometer using its 136-channel digital correlator at IBM or at UNLV in a home-built system that has been described in some detail earlier.[17] The UNLV system was modified by the substitution of a 136-channel Brookhaven correlator for the earlier Langley–Ford or Saicor correlators. All autocorrelation functions measured were "unclipped".

$\bar{M}_W$ and A_2 values for PαMS were determined from the concentration dependence of the absolute intensity of scattered light, while $\bar{M}_W/\bar{M}_N$ values were determined by size-exclusion chromatography (SEC) in tetrahydrofuran. Values of $\bar{M}_W$ and A_2 were obtained by extrapolation of measurements at 4–6 concentrations to infinite dilution, obtaining $\bar{M}_W$ and A_2 from the intercept and slope of a square-root plot

$$\left(\frac{Kc}{R_0}\right)^{1/2} = \left(\frac{1}{\bar{M}_W}\right)^{1/2}[1 + A_2\bar{M}_W^{1/2}c] \qquad (10)$$

where the subscript 0 indicates extrapolation to zero scattering angle and R_θ at 4° scattering angle is taken as equivalent to R_0. The constant $K = 4\pi n^2(dn/dc)^2/\lambda^4 N_A$. Experimental data in cyclohexane at 50 °C are shown in Figures 1 and 2. The values of $\bar{M}_W$ reported in Table I are the averages of the light-scattering results in cyclohexane and toluene and the SEC results. The refractive index increments (dn/dc) measured were 0.194 and 0.124 mL/g for cyclohexane and toluene, respectively. These values were obtained at 30 °C and λ = 632.8 nm using a Chromatix KMX-16. This dn/dc in toluene is significantly larger than that we reported in an earlier study.[16] We believe the earlier value to be in error, as has also been suggested recently by Lindner et al.[19] The A_2 and $\bar{M}_W$ values of samples 1–7 measured in toluene were taken from the earlier study and have been corrected to reflect the change in dn/dc.

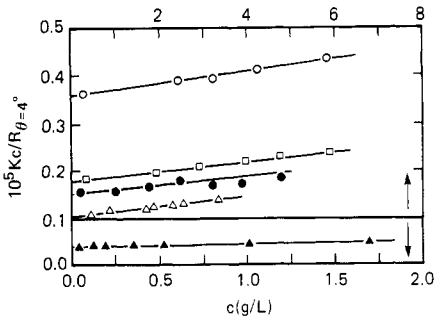

Figure 1. $Kc/R_{\theta=4°}$ versus concentration for PαMS samples 5–9 in marginal solvent (cyclohexane at 50 °C). By sample number: ○, 5; □, 6; ●, 7; △, 8; ▲, 9.

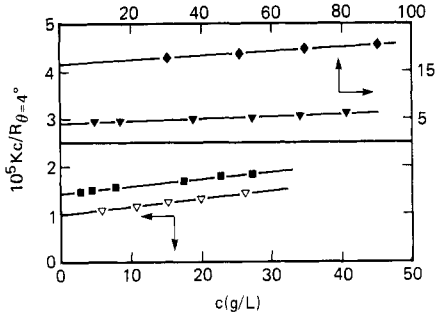

Figure 2. $Kc/R_{\theta=4°}$ versus concentration for PαMS samples 1–4 in marginal solvent (cyclohexane at 50 °C). By sample number: ♦, 1; ▼, 2; ■, 3; ▽, 4.

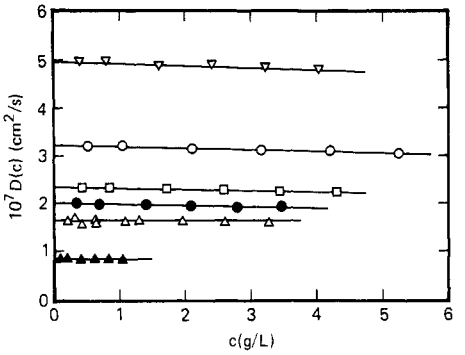

Figure 3. $D(c)$ versus c for PαMS samples 4–9 in marginal solvent (cyclohexane at 50 °C). Symbols denote sample numbers as in Figures 1 and 2.

R_H and k_D^c values were determined using cumulant analyses of scattered light autocorrelation functions.[20] In the cumulant expansion, deviations of the correlation function from a single exponential are approximated by a series expansion

$$\ln|g^{(1)}(q,t)| = -\bar{\Gamma}_1 t + \mu_2 t^2/2 + \ldots \qquad (11)$$

in powers of the delay time t. The scattering vector $q = (4\pi n/\lambda_0)\sin(\theta/2)$ with λ_0 the wavelength of light, 632.8 nm in a vacuum, and n the refractive index of the solvent.

$$b^{1/2}|g^{(1)}(t)| = [g^{(2)}(t) - 1]^{1/2} \qquad (12)$$

where $g^{(2)}(t)$ is the normalized measured intensity time correlation function $(C(t)/B)$, and b is an optical factor related to the number of coherence areas viewed by the detector. The base line B was determined by an average of 4 channels delayed to 1024 times the last correlator channel. Measured and calculated base lines agreed within 0.02%. The first cumulant $\bar{\Gamma}_1$

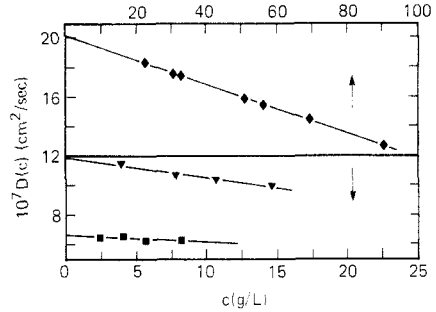

Figure 4. $D(c)$ versus c for PαMS samples 1–3 in marginal solvent (cyclohexane at 50 °C). Symbols denote sample numbers as in Figure 2.

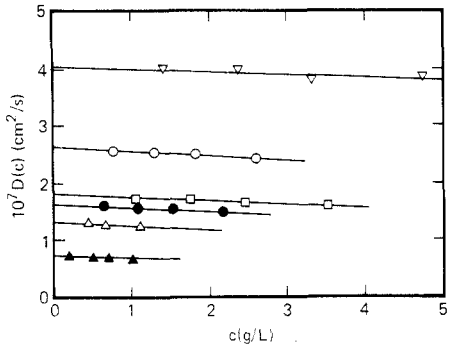

Figure 5. $D(c)$ versus c for PαMS samples 4–9 at T_θ (cyclohexane at 35 °C). Note that the slopes are the same. Symbols denote sample numbers as in Figures 1 and 2.

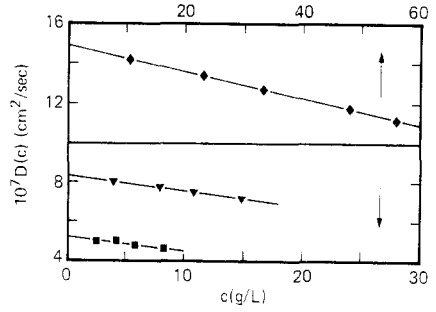

Figure 6. $D(c)$ versus c for PαMS samples 1–3 at T_θ (cyclohexane at 35 °C), as determined by PCS. Note that the slopes are the same (two scales are used). Symbols denote sample numbers as in Figure 2.

has been shown by Koppel to lead to the z-average diffusion coefficient in the limit of infinite dilution[20]

$$\bar{\Gamma}_1 = D_z q^2 \tag{13}$$

The normalized second cumulant, $\mu_2/\bar{\Gamma}_1^2$, was 0.07 or less for these samples reflecting their narrow molecular weight distribution (see Table I). All but the lowest M sample had polydispersity indices $\bar{M}_W/\bar{M}_n$ of <1.2.

III. Results and Discussion

Marginal solvent (cyclohexane at 50 °C) static and dynamic light-scattering results for samples 1–9 are presented in Figures 1 and 2 and Figures 3 and 4, respectively. Θ solvent (cyclohexane at 35 °C) dynamic light-scattering results for samples 1–9 are presented in Figures 5 and 6. Computation of k_D^φ requires measurement of $\bar{M}_W$, k_D^c, and R_H

$$k_D^\varphi = (M/N_A V_H) k_D^c \tag{14}$$

setting $M = \bar{M}_W$. Computation of X then requires measurement of A_2 and R_H as discussed earlier. $\bar{M}_W$ and the polydispersity results are presented in Table I, and

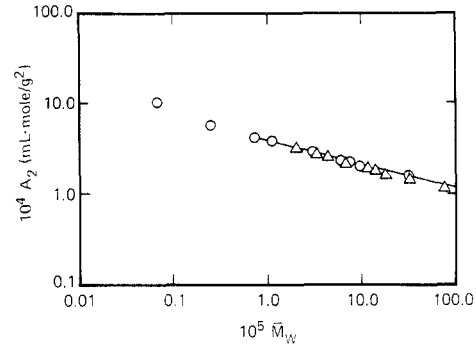

Figure 7. A_2 as a function of M_W ror PαMS samples 1–9 in good solvent (toluene, 25 °C) (○). Also included are measurements made by Kato et al.[12] (△). Equation 16 in the text presents the power law fit for PαMS samples with $\bar{M}_W > 10^5$.

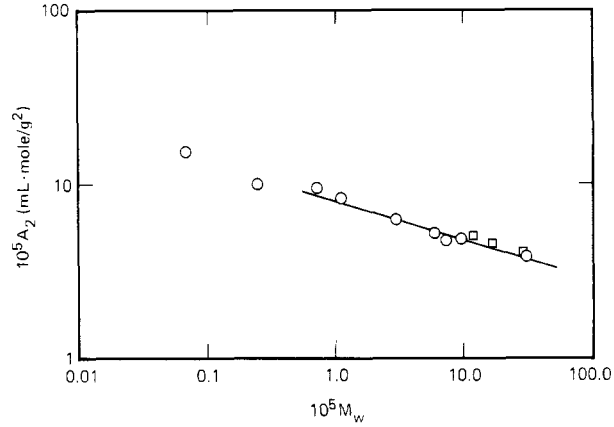

Figure 8. A_2 as a function of M_W for PαMS samples 1–9 in marginal solvent (cyclohexane at 50 °C) (○). Also included are measurements made by Kato et al.[14] (□). Equation 15 in the text presents the power law fit for PαMS samples with $\bar{M}_W > 10^5$.

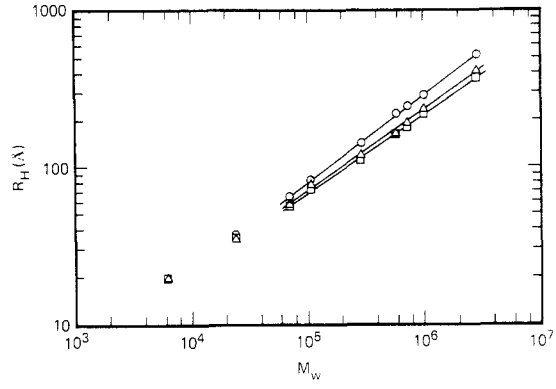

Figure 9. R_H as a function of M_W for PαMS samples 1–9 in good (○), marginal (△), and Θ solvents (□). Power law fit results for $\bar{M}_W > 10^5$ are presented in eqs 17–19 in the text.

A_2 results for toluene at 25 °C and cyclohexane at 50 °C are presented in Figures 7 and 8 and Tables II and IV. The results of the present study are seen to be very consistent with earlier measurements by Kato et al., of high molecular weight, narrow distribution, PαMS in toluene at 25 °C[12] (Figure 7) and in cyclohexane at 50 °C[15] (Figure 8). For $\bar{M}_w > 50\,000$ (see below), that is, for samples 3–9, fits to the combined results yield

$$A_2 = (11 \pm 2) \times 10^{-4} M_W^{-0.23\pm0.03} \text{ (mL·mol/g}^2\text{)} \tag{15}$$

and

$$A_2 = (9 \pm 2) \times 10^{-3} \bar{M}_W^{-0.28\pm0.01} \text{ (mL·mol/g}^2\text{)} \tag{16}$$

Table II
PαMS $T \gg \Theta$ Results (Toluene at 25 °C)

sample no.	$10^4 A_2$, cm³/g ± 10%	$\tilde{S}/R_H$ ± 10%	$10^7 D_0$, cm²/s ± 2%	R_H, Å ± 2%	$k_D{}^c$, cm³/g ± 14%	$k_D{}^\varphi$ ± 20%
1	10.2	0.79	19.55	20.1	1.12	0.34
2	5.63	0.88	10.67	36.8	4.63	0.90
3	4.13	0.92	6.10	64.4	13.5	1.42
4	3.78	0.93	4.76	82.5	19.7	1.56
5	2.89	0.95	2.77	142	46.0	1.72
6	2.30	0.91	1.80	218	88.9	1.98
7	2.23	0.93	1.61	244	105	2.03
8	1.98	0.94	1.36	289	132	2.21
9	1.56	0.97	0.805	521	288	2.34

Table III
PαMS $T = \Theta$ Results (Cyclohexane at 35 °C)

sample no.	$10^7 D_0$, cm²/s ± 3%	$10^6(-\delta D/\delta c)$, cm⁵/g·s ± 13%	R_H, Å ± 2%	$-k_D{}^c$, cm³/g ± 14%	$-k_D{}^\varphi$ ± 20%
1	14.95	6.8	19.5	4.5	1.5
2	8.22	7.6	35.1	9.1	2.05
3	5.26	7.38	55.8	14.1	2.28
4	4.07	5.23	71.8	15.9	2.15
5	2.63	7.66	111	24.0	1.96
6	1.81	6.01	161	35.8	1.98
7	1.63	6.77	179	39.8	1.97
8	1.35	7.4	216	48.0	2.05
9	0.818	7.1	369	86.8	1.98

Table IV
PαMS $T > \Theta$ Results (Cyclohexane at 50 °C)

sample no.	$10^5 A_2$, cm³/g ± 30%	$\tilde{S}/R_H$ ± 10%	$10^7 D_0$, cm²/s ± 4%	$10^6(-\delta D/\delta c)$, cm⁵/g·s ± 30%	R_H, Å ± 3%	$-k_D{}^c$, cm³/g ± 15%	$-k_D{}^\varphi$ ± 20%
1	16	0.44	20.0	8.2	19.6	4.1	1.36
2	10	0.52	11.1	6.1	35.3	5.5	1.22
3	9.5	0.61	6.61	4.9	59.4	7.4	0.99
4	8.4	0.59	5.00	4.72	78.5	9.44	1.02
5	6.3	0.67	3.23	3.23	121	10.0	0.611
6	5.2	0.72	2.35	2.37	167	10.1	0.415
7	4.8	0.70	2.02	2.25	194	11.1	0.404
8	4.9	0.73	1.68	0.498	234	2.96	0.092
9	3.9	0.76	0.876	≈0	419	≈0	≈0

Table V
PαMS $T < \Theta$ Results (Cyclohexane at 25 °C)

sample no.	$-10^5 A_2$,[a] cm³/g·mol ± 30%	$-\tilde{S}$, Å ± 10%	$10^7 D_0$, cm²/s ± 3%	R_H, Å ± 3%	$-k_D{}^c$, cm³/g ± 15%	$-k_D{}^\varphi$, ± 20%
1		6	11.9	20.4	4.8	1.4
2		16	7.45	32.6	12.3	3.5
3		32	4.44	54.7	19.2	3.3
4	7.0	42	3.65	66.6	32.4	4.7
5		84	2.30	106	51.5	5.0
6		133	1.63	149	72.6	4.6
7		154	1.44	160	82.2	4.9
8	7.3	195	1.26	193	94.0	5.2

[a] Unless an experimental A_2 is listed, a value of -7×10^{-5} was used to calculate $\tilde{S}$; see text.

for cyclohexane at 50 °C (eq 15) and toluene at 25 °C (eq 16). The toluene data in Figure 7 show the upward curvature at low M as has been reported by others for polystyrene in good solvents.[21-24] In contrast, current theories for flexible polymers predict a downward curvature at low M. Huber et al.[21] propose the contribution of chain stiffness at low M as an explanation for this behavior and for a similar upturn in R_H discussed below. The molecular weight dependence of A_2 in the marginal solvent (Figure 8, eq 15) is similar to that observed in toluene. While an exponent of $-1/5$ is expected in good solvents (hard-sphere approximation), recent theories predict a more pronounced molecular weight dependence in poor solvents, with an exponent near $-1/2$.[25,26] This increased molecular weight dependence was not observed here nor has it been reported experimentally to our knowledge. A negligible molecular weight dependence of A_2 for sub-Θ solvents has been observed as discussed below. Accurate measurements of A_2 in poor solvents are very difficult and more studies are needed.

PCS R_H and $k_D{}^c$ results for samples 1–9 are presented in Tables II–V. Included in Table II are results for samples 1–7 from an earlier light-scattering study of PαMS in toluene,[16] and included in Table V are results from samples 4–9 from an earlier study of PαMS in cyclohexane below T_Θ.[17] R_H versus $\bar{M}_W$ plots for PαMS in good, marginal, and Θ solvents are presented for samples 1–9 in Figure 9.

The upward curvature of the three plots in Figure 9, at least until a molecular weight around 10^5, is evident. Power law fits used to characterize the A_2 and R_H dependences were therefore restricted to samples 3–9 having $\bar{M}_w > 50\,000$. These fits yield

$$R_H(\bar{M}_W) = (0.116 \pm 0.0007)\bar{M}_W{}^{0.566\pm0.005} \text{ (good solvent)} \quad (17)$$

$$R_H(\bar{M}_W) = (0.191 \pm 0.053)\bar{M}_W{}^{0.514\pm0.023} \text{ (marginal solvent)} \quad (18)$$

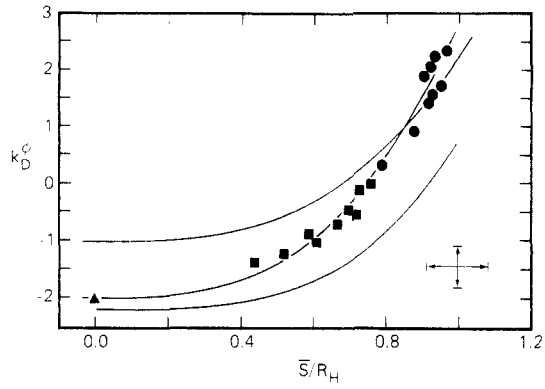

Figure 10. $k_D^{\varphi}(X)$ versus $X \equiv \bar{S}/R_H$ results for PαMS samples 1–9 in good (●), marginal (■), and Θ solvents (▲). Error bars correspond to typical uncertainties in k_D^{φ} and X. Details are presented and discussed in the text.

and

$$R_H(\bar{M}_W) = (0.199 \pm 0.033)\bar{M}_W^{0.505\pm0.013} \text{ (Θ solvent)} \quad (19)$$

with R_H in angstroms. Although the focus of this study is on PαMS–PαMS interactions in dilute solution, PαMS intrapolymer behavior, as exhibited in the hydrodynamic results presented in Figure 9, merits further comment. The coalescence of chain hydrodynamic radii around $\bar{M}_W$ = 20 000 reveals the insensivity of chain hydrodynamic volume to solvent quality for sufficiently small chains. At these low molecular weights the number of long-range excluded-volume interactions per chain is small and has little effect on the hydrodynamic size. In addition, R_H is less sensitive to the external portions of the polymer coil where the excluded volume effects are most evident. In contrast, the root-mean-square radius of gyration R_G, is very sensitive to long-range interactions, and significant differences between good and poor solvents can be observed for much lower values of M.[21] Chain hydrodynamic radii for $\bar{M}_W \approx 20\,000$ are distinctly larger than those expected from extrapolation of high molecular weight PαMS R_H versus $\bar{M}_W$ fits. Both types of behavior were recently observed and carefully analyzed by Huber et al.[21] in their study of the hydrodynamic and thermodynamic behavior of linear polystyrene with $M < 30\,000$. Huber et al. consider both the contributions of non-Gaussian chain statistics (stiffness) and also hydrodynamic effects. They concluded that the short-chain effects on the translational friction coefficient could be well described by either the standard Kirkwood theory including the first free-draining term or by the Yamakawa–Fujii theory for wormlike chains.

The results of the PαMS–PαMS interaction study are summarized in the $k_D^{\varphi}(X)$ versus X plot presented in Figure 10. A compendium of results from light-scattering studies similar to that presented here for both polystyrene and PαMS reveals considerable scatter in the $k_D^{\varphi}(X)$ versus X data.[9,10] To get a better feel for the origins of this scatter, the results of this study include estimates of uncertainty for both k_D^{φ} and for X and these uncertainties appear in Tables II, IV, and V. Representative horizontal and vertical error bars for typical uncertainties are shown in Figure 10. Uncertainties in k_D^{φ} were computed by compounding k_D^c uncertainties, via eq 14, with conservative uncertainties estimated for R_H of 7% and for $\bar{M}_W$ of 10%. At T_θ, $\partial D/\partial c = D_0 k_D^c$ and is independent of molecular weight (see eq 1, Figure 5 and refs 9, 27, and 28). Thus values of $D_0 k_D^c$ averaged for samples 4–9 yield a mean value with a small uncertainty. This mean value with its small uncertainty was used along with corresponding D_0 values, also having small uncertainties, to calculate individual k_D^c and k_D^{φ} values (Table III). The simple averaged k_D^{φ} for samples 4–9 is then −2.02 ± 0.07. Except at T_Θ, X uncertainties were calculated assuming 15% uncertainties for A_2. Since A_2 was determined to vanish at (T_θ = 34.5 ± 0.5 °C), the uncertainty in X at $X = 0$ is particularly small. The value of T_Θ determined here is in excellent agreement with that found earlier by Kato et al.[12] for high molecular weight PαMS in cyclohexane. Clearly, k_D^{φ} and X uncertainties above T_θ resulting from the propagation of uncertainties in the measured parameters used to calculate them are consistent with the rather large scatter observed in the data from earlier studies.

The curves in Figure 10 represent the theories of Yamakawa[4] (upper curve), of Pyun and Fixman[7] (lower curve), and of Akcasu.[8-10,29] In the Yamakawa treatment

$$k_s^{\varphi}(X) = 4.8X^3 + 1 \quad (20)$$

while in the P–F treatment

$$k_s^{\varphi}(X) = -\kappa(A) + 7.16 \quad (21)$$

with the relation between A and X described below.

As reported in earlier studies,[9,16,27,28] the good solvent results of this study were more consistent with the Yamakawa treatment while the poor solvent results were adequately described by the treatment of Pyun and Fixman. Neither the Yamakawa nor the original P–F treatments adequately describes polymer–polymer interactions in solution over the solvent quality range from poor through marginal to good. Recent modification of the P–F treatment has however resulted in an improved description of this behavior[30-32] but has led to some confusion as to which version of the P–F theory is being used in a given study. In an attempt to avoid such confusion, the data of this study are being compared to the "original" version, which is now specified in a brief outline. In this outline, the formulation of the P–F results as presented by Akcasu[10] has been employed.

Pyun and Fixman modeled binary clusters of spherically symmetric interpenetrating polymers as ellipsoids after having first considered them as overlapping spheres whose segment densities have managed to remain uniform. One length, R_H, is used to characterize both individuals as well as clusters. For prolate ellipsoids in particular (Figure 10), $\kappa(A)$ in eq 21 is written

$$\kappa(A) = 24\int_0^1 \left\{\frac{\ln\,[1 + x + (2x + x^2)^{1/2}]}{(2x + x^2)^{1/2}} - 1\right\} \times x^2 e^{-A(1-x)^2(2+x)}\,dx \quad (22)$$

with R the center-of-mass separation between polymer pairs and $x \equiv R/2R_H$. In turn, X may be written[10]

$$X = \{3\int_0^1 x^2[1 - e^{-A(1-x)^2(2+x)}]\,dx\}^{1/3} \quad (23)$$

For the uniform density sphere model,[4] X and A may be related by the function $h_0(A)$ reflecting the molecular weight dependence

$$h_0(A) = \frac{12}{A}\int_0^1 x^2[1 - e^{-A(1-x)^2(2+x)}]\,dx \quad (24)$$

with $h_0(A)$ developed in ref 4, for example. Combining eqs 23 and 24, the relation between X and A (see eq 21) is found to be

$$4X^3 = Ah_0(A) \quad (25)$$

X and $k_D^{\varphi}(X)$ are then calculated as functions of A using eqs 8 and 21–23. The result is presented as the lower curve in Figure 10. Note that $X_{max} = 1$ and $k_D^{\varphi}(X_{max}) = 0.84$ in the original P–F treatment.

The results of any theoretical treatment of k_s^{φ} for linear, flexible polymer chains depend sensitively on the details of the polymer segment distribution in a binary cluster; this sensitivity is particularly important near T_θ where significant interpenetration occurs. Difficulties associated with model dependent sensitivity are avoided here by employing a semiempirical fit to the $k_D^{\varphi}(X)$ versus X data based upon recent theoretical work by Akcasu[10] and Akcasu and co-workers.[8,9,29] In addition to providing a good fit to the observed PαMS results over the entire range of X probed, including sub-Θ behavior, the results of the fit are both interesting and instructive.

$k_s^{\varphi}(X)$ may be written[29] as

$$k_s^{\varphi}(X) = 6Y^2 \tag{26a}$$

so

$$k_D^{\varphi}(x) = 8X^3 - 6Y^2 \tag{26b}$$

with $Y = Y(X)$ determined here empirically. In earlier work, for example, it was shown that, in good solvents, $Y(X) = X$.[8] More generally, Y may be expressed in terms of the first moment of the pair correlation function $g(R)$ of two chains with a center-of-mass separation R:

$$Y^2 = \frac{1}{2R_H^2}\int_0^\infty R[1 - g(R)]\, dR \tag{27}$$

Thus, Y may be viewed as a polymer excluded surface area term, while X, the associated excluded-volume term, is expressed in terms of the second moment of $g(R)$

$$X^3 = \frac{3}{8R_H^3}\int_0^\infty R^2[1 - g(R)]\, dR \tag{28}$$

with R as in eqs 22–24. Thus, X must vanish at T_θ while Y remains finite. Note that eq 23 follows from eq 28 with $g(R)$ expressed in terms of a uniform density sphere model with the cutoff in R given by $R = 2R_H$. Recent Monte Carlo calculations by Olaj and co-workers[34] of two chains in Θ and athermal solvents provide estimates for $g(R)$. These results suggest that $X \cong Y$ in athermal solvents, as suggested by Akcasu and Benmouna based on the hard-sphere potential. The computer calculations also show a concentration dependence of the average chain dimensions even in Θ solvents. This increase in chain dimensions resulting from a binary encounter has been suggested as the origin of the nonvanishing k_D in Θ solvents.[10]

In Figure 10, it is seen that k_D^{φ} increases smoothly and monotonically with increasing X. This smooth increase of k_D^{φ} with solvent quality illustrates the gradual transition in the system from poor through marginal to good solvent behavior. A Θ "plateau" is evident in the vicinity of $X = 0$. A unique feature of the Akcasu form for k_D^{φ} is that both the temperature dependence and molecular weight dependence are reflected in the parameter X. Thus, in Figure 10, decreasing values of X for lower molecular weight samples in the good solvent toluene merge smoothly into the highest molecular weight samples in the marginal solvent (cyclohexane at 50 °C), forming a continuous curve. For the lowest M sample (no. 1), a positive A_2 was measured even at $T_\theta = 34.5$ °C in cyclohexane. The negative value of k_D^{φ} was also smaller than was observed for the higher M samples at T_θ (see Table III). This is consistent with some theoretical predictions and some experimental data.[39] We have not included this point in Figure 10 due to the large uncertainty in the A_2 value. However, it should be noted that this behavior is consistent with the θ plateau in Figure 10 where k_D^{φ} is unchanged from the θ value for small positive X. In this region, although $A_2 > 0$ and thus $X > 0$, the expansion factor, at least for hydrodynamic measurements, is very close to unity.

The form for $k_s^{\varphi}(X)$ in $k_D^{\varphi}(X)$ was chosen using the expression of Akcasu and Benmouna, $k_D^{\varphi} = 8X^3 - 6Y^2$, as a guide. This illustrates clearly the competition between the thermodynamic first term reflecting excluded-volume behavior and the hydrodynamic second term reflecting the friction coefficient and of opposite sign. Dimensionality considerations and a comparison of the integral equations for X^3 and Y^2 (eqs 27 and 28) suggests $Y^2(X) \sim X^3$. Thus

$$Y(X) = (A + BX^3)^{1/2} \tag{29}$$

was chosen. A polynomial least-squares fit to the data for $X \geq 0$ yields

$$Y(X) = (0.33 + 0.53X^3)^{1/2} \tag{30}$$

so that

$$k_s^{\varphi}(X) = 3.2X^3 + 2.0 \tag{31a}$$

and

$$k_D^{\varphi}(X) = 4.8X^3 - 2.0 \tag{31b}$$

providing a good fit to the data across the range $0 \leq X \lesssim 1$ (middle curve in Figure 10). This result is similar to that derived earlier by Yamakawa (cf. eq 20, Figure 10) for which $k_D^{\varphi}(X) = 3.2X^3 - 1$. Near equivalence of $\bar{S}$ and R_H has been observed for flexible polymers in good solvents, so that the athermal value of X is expected to be near unity, as observed here.

These results are consistent with a number of predictions. From the results (Table II and Figure 10), $k_D^{\varphi}(X) \simeq 2$ in good solvent, in reasonable accord with the value of 1.74 predicted by Yamakawa (eqs 8 and 20) and in good agreement with the hard-sphere prediction of 2 by Altenburger and Deutch[33] as well as Akcasu's prediction of 2 for polymer coils. The possibility that X may be somewhat greater in the good solvent limit than that observed here and the consequences this greater X has on k_D^{φ} have been discussed in some detail in ref 10. For $X = 1$, $Y = 0.93$ (eq 30) in good agreement with Akcasu's prediction that $X \simeq Y$ in good solvent.[8,29] For marginal solvent (Table IV and Figure 10), $k_D^{\varphi} = 0$ at $X = 0.75$, again in good agreement with theory. Note that k_D^{φ} is actually zero, within experimental error, for PαMS sample 9 in cyclohexane at 50 °C. At T_Θ, $k_D^{\varphi} = -2.02 \pm 0.07$ (Table III), and using eq 30, Y is calculated to be 0.57. This nonzero value for Y may be compared with the first moment of the pair distribution function $g(R)$ obtained from the Monte Carlo calculations of Olaj et al.[34] Finite and positive values of the first moment, as obtained here and by Akcasu et al. using the data of Olaj et al. are in contrast to the conventional smoothed density models (e.g., Flory–Krigbaum[40]) where the first as well as the second moments are expected to vanish at T_θ.

Measurements of all but the highest molecular weight sample were also carried out at 25 °C in cyclohexane to investigate the behavior of k_D below T_θ. These measurements were more difficult due to incipient phase separation. However, as reported in an earlier study, the PαMS samples remain in solution at significantly lower temper-

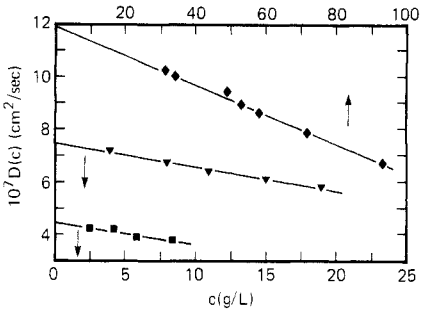

Figure 11. $D(c)$ versus c for PαMS samples 1–3 below T_θ (cyclohexane at 25 °C). Symbols denote sample numbers as in Figure 2.

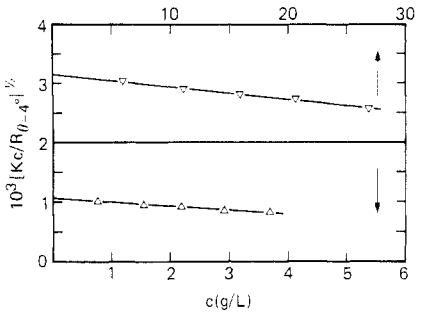

Figure 12. $[Kc/R_{\theta=4^\circ}]^{1/2}$ versus c for PαMS samples 4 and 8 below T_θ (cyclohexane at 25 °C). Symbols denote sample numbers as in Figures 1 and 2.

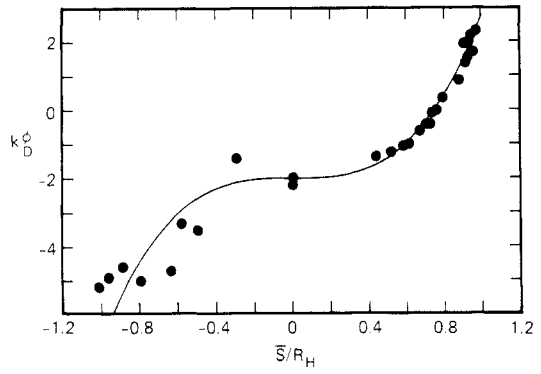

Figure 13. $k_D{}^\varphi(X)$ versus $X \equiv \bar{S}/R_H$ results for PαMS samples 1–9 illustrating sub-Θ behavior. Details are presented and discussed in the text.

atures than is observed for polystyrene and are thus excellent candidates for studies below T_θ such as the collapse transition. Values of D_0, $k_D{}^c$, and R_H are listed in Table V; those of samples 4–7 were reported earlier.[17] The concentration dependence of $D(c)$ is shown in Figure 11 for samples 1–3.

Tong et al.[35] have measured A_2 of polystyrene in cyclohexane at temperatures below T_θ and shown that in this region A_2 appears independent of M. This unexpected result has also been obtained by Perzynski et al.[36] and also for polyisoprene in dioxane below T_Θ.[37,38] Measured A_2 values for samples 4 and 8 of PαMS in cyclohexane at 25 °C were the same within the experimental uncertainty despite 1 order of magnitude difference in $\bar{M}_W$ for these samples, as may be seen in Figure 12 and Table V. A range of values of from $-(5–9) \times 10^{-5}$ for A_2 produces only a 10% variation in $\bar{S}$. For these reasons, a value of -7×10^{-5} was used for A_2 to estimate $\bar{S}$ for all samples. It may be seen from Table V and Figure 13 that $k_D{}^\varphi$ continues to become more negative as X becomes more negative, approaching −5 for the higher molecular weight samples 4–8. Figure 13 shows the entire range of solvent quality investigated including the sub-Θ region where $X < 0$. Within the large uncertainty in the data below T_Θ it may be seen that the values measured for $k_D{}^\varphi$ are not inconsistent with eq 31. The Θ region defined by the plateau in Figure 10 continues for small negative values of X. At low molecular weights the small number of long-range interactions minimizes chain shrinkage below T_θ. This is also seen in the nearly constant value for R_H obtained for the lowest M sample, independent of temperature. The empirical expression obtained above (eq 31a) may be used to calculate the value of $X = -0.85$, where $k_s{}^\varphi$ may be expected to vanish. Substituting this value for X into eq 8 above yields $k_D{}^\varphi = -4.9$ in this region, very consistent with the experimental values measured for highest molecular weight samples 4–8. Pyun and Fixman[8] predicted that $k_s{}^\varphi$ would vanish at $A \cong -1$, corresponding to $X = -0.71$, which is also very consistent with the results in Table V. Thus, the concentration dependence of the friction coefficient (sedimentation constant, tracer diffusion) is seen to vanish only nearly 10 deg below T_θ.

Acknowledgment. We benefited from conversations concerning this work with A. Z. Akcasu and W. Burchard as well as the technical assistance of H. Knocke, T. Gibbons, A. R. Ellis, and B. J. Corrado and the generous donation of PαMS samples 8 and 9 by L. Rosen of the Pressure Chemical Co. Acknowledgment is also made by J.C.S. to the donors of the Petroleum Research Fund, administered by the Americal Chemical Society, for partial support of this research.

References and Notes

(1) Huglin, M. B. *Light Scattering from Polymer Solution*; Academic Press: London, 1972.
(2) Chu, B. *Laser Light Scattering*; Academic Press: New York, 1974.
(3) Berne, B. J.; Pecora, R. *Dynamic Light Scattering with Applications to Chemistry, Biology and Physics*; Wiley: New York, 1976.
(4) Yamakawa, H. *Modern Theory of Polymer Solutions*; Harper and Row: New York, 1971.
(5) Flory, P. J. *Principles of Polymer Chemistry*; Cornell University Press: Ithaca, NY, 1953.
(6) Tanford, C. *Physical Chemistry of Macromolecules*; Wiley: New York, 1963.
(7) Pyun, C. W.; Fixman, M. *J. Chem. Phys.* **1964**, *41*, 935.
(8) Akcasu, A. Z.; Benmouna, M. *Macromolecules* **1978**, *11*, 1193.
(9) Han, C. C.; Akcasu, A. Z. *Polymer* **1981**, *22*, 1165.
(10) Akcasu, A. Z. *Polymer* **1981**, *22*, 1169.
(11) Lyerla, J.; Horikawa, T.; Fleming, W., IBM Research Laboratory, San Jose, CA, unpublished results.
(12) Kato, T.; Miyaso, K.; Noda, I.; Fujimoto, T.; Nagasawa, M. *Macromolecules* **1970**, *3*, 777.
(13) Brownstein, S.; Bywater, S.; Worsfold, D. J. *Makromol. Chem.* **1961**, *48*, 127.
(14) Cotts, P. M. *Macromolecules* **1986**, *19*, 488.
(15) Kato, T.; Miyaso, K.; Nagasawa, M. *J. Chem. Phys.* **1968**, *72*, 2161.
(16) Selser, J. C. *Macromolecules* **1981**, *14*, 346.
(17) Selser, J. C. *Macromolecules* **1985**, *18*, 587.
(18) Selser, J. C. *Macromolecules* **1979**, *12*, 909.
(19) Lindner, J. S.; Wilson, W. W.; Mays, J. W. *Macromolecules* **1988**, *21*, 3304.
(20) Koppel, D. E. *J. Chem. Phys.* **1972**, *57*, 4814.
(21) Huber, K.; Bantle, S.; Lutz, P.; Burchard, W. *Macromolecules* **1985**, *18*, 1461.
(22) Fujita, H. *Macromolecules* **1988**, *21*, 179.
(23) Fujita, H.; Norisuye, T. *Macromolecules* **1985**, *18*, 1637.
(24) Miyaki, Y.; Einaga, Y.; Fujita, H. *Macromolecules* **1978**, *11*, 1180.
(25) Sanchez, I. C.; Lohse, D. J. *Macromolecules* **1981**, *14*, 131.
(26) Rabin, Y. *J. Chem. Phys.* **1983**, *79*, 3988.
(27) Han, C. C. *Polymer* **1979**, *20*, 259.
(28) Gulari, E.; Gulari, E.; Tsunashima, Y.; Chu, B. *Polymer* **1979**, *20*, 347.

(29) Akcasu, A. Z.; Hammouda, B.; Lodge, T. P.; Han, C. C. *Macromolecules* **1984**, *17*, 759.
(30) Van Den Berg, J. W. A.; Jamieson, A. M. *J. Polym. Sci., Polym. Phys. Ed.* **1983**, *21*, 2311.
(31) Tsunashima, Y.; Nemoto, N. *Macromolecules* **1983**, *16*, 1941.
(32) Huber, K.; Burchard, W.; Akcasu, A. Z. *Macromolecules* **1985**, *18*, 2743.
(33) Altenburger, A. R.; Deutch, J. M. *J. Chem. Phys.* **1973**, *59*, 89.
(34) Olaj, O. F.; Lantschbauer, N.; Pelinka, K. H. *Macromolecules* **1980**, *13*, 299.
(35) Tong, Z.; Ohashi, S.; Einaga, Y.; Fujita, H. *Polym. J.* **1983**, *11*, 835.
(36) Perzynski, R.; Delsanti, M.; Adam, M. *J. Phys.* **1987**, *48*, 115.
(37) Takano, N.; Einaga, Y.; Fujita, H. *Polym. J.* **1985**, *17*, 1123.
(38) Fujita, H. *Macromolecules* **1988**, *21*, 179.
(39) Huber, K.; Stockmayer, W. H. *Macromolecules* **1987**, *20*, 1400.
(40) Flory, P. J.; Krigbaum, W. R. *J. Chem. Phys.* **1950**, *18*, 1086.

Registry No. Poly(α-methylstyrene), 25014-31-7.

Cyclization Dynamics of Flexible Polymers. Numerical Results from Brownian Trajectories

José L. Garcia Fernández, Antonio Rey, Juan J. Freire,* and Inés Fernández de Piérola

Departamento de Quimica Fisica, Facultad de Ciencias Quimicas, Universidad Complutense, 28040 Madrid, Spain. *Received July 6, 1989; Revised Manuscript Received October 13, 1989*

ABSTRACT: Brownian trajectories of Gaussian chains of different lengths, generated with fluctuating hydrodynamic interactions in previous work, have been analyzed to study the rate constants of cyclization processes. The cyclization constants are compared with those previously calculated by Perico and Cuniberti through the approximate Wilemski–Fixman theory (in which hydrodynamic interactions are preaveraged). A significant disagreement is found between these theoretical and simulation values. The disagreement increases for increasingly stiffer chains and does not seem to be mainly caused by the preaveraging approximation. The simulation values for cyclization are in agreement with rate constants obtained from experimental work, but our decyclization constants are considerably higher than the experimental data.

Introduction

The kinetics of intrachain reactions under conditions of diffusion control is an interesting problem directly connected with the intramolecular dynamics of polymer chains in solution.[1] A theoretical description of this problem has been provided by Wilemski and Fixman[2] (WF). This theory can be applied to polymer models as the popular Rouse–Zimm model[3,4] (i.e., the bead-and-spring model with preaveraged hydrodynamic interactions). Detailed calculations for this model have been reported by Perico and Cuniberti[5] (PC). However, the WF theory includes some additional approximations since it is based on the use of a nonconservative perturbation in the time distribution function of the chain. WF consider that the distribution function of the polymer in the reaction region is in equilibrium. This approximation has been checked by Doi[6] for a harmonic dumbbell and he found that the exact results deviate from the WF prediction by up to 20%. Also, there has been further theoretical work[7–10] that points out different problems related with the WF approach.

Given this situation, it seems desirable to check the theory with simulation results. In this work we report calculations performed from Brownian dynamics trajectories previously obtained for linear chains of different lengths. These trajectories were used elsewhere to study other equilibrium and dynamic properties.[11] The trajectories were generated according to a bead-and-spring model consistent with the PC calculations. However, we introduced in this model an adequate nonpreaveraged description of hydrodynamic interactions. This way, our results are free of the different approximations contained in the WF theory. The discussion of differences between the simulation and theoretical values and the comparison with some experimental data are also included.

Model, Methods, and Numerical Results

We model the polymer molecules as bead-and-spring chains composed of $N + 1$ identical beads. Then, the intramolecular force $\mathbf{F}_j$ exerted by the neighbors of bead j is given by

$$\mathbf{F}_j = (3k_BT/b^2)(\mathbf{AR})_j \tag{1}$$

where k_BT is the Boltzmann factor, b is the bead statistical length, $\mathbf{R}$ contains the position vectors of the different units, $\mathbf{R}_i$, and $\mathbf{A}$ is the Rouse connectivity matrix.[3,4] Excluded-volume forces are not considered so that the chain equilibrium properties are consistent with the Gaussian chain model.

The Stokes radius of the beads, σ, that determines the frictional force associated with their motions is given in terms of the parameter h^*

$$h^* = (3/\pi)^{1/2}(\sigma/b) \tag{2}$$

for which we have set the value $h^* = 0.25$. Hydrodynamic interactions are described by means of the Rotne–Prager[12]–Yamakawa[13] tensor

$$\mathbf{D}_{ii} = (k_BT/\xi)\mathbf{I}$$

($\mathbf{I}$ is a 3×3 unit tensor)

$$\mathbf{D}_{ij} = (3k_BT/4\xi)(\sigma/R_{ij})[\mathbf{I} + \mathbf{R}_{ij}\mathbf{R}_{ij}/R_{ij}^2 + (2\sigma^2/3R_{ij}^2)(\mathbf{I} - 3\mathbf{R}_{ij}\mathbf{R}_{ij}/R_{ij}^2)] \quad \text{if } R_{ij} \geq 2\sigma$$

0024-9297/90/2223-2057$02.50/0